Available online at www.sciencedirect.com
ScienceDirect
Journal of Power Sources 179 (2008) 220–231
JOURNAL OF POWER SOURCES
www.elsevier.com/locate/jpowsour

Transient response of high temperature PEM fuel cell

J. Peng *, J.Y. Shin, T.W. Song

Energy and Environment Laboratory, Samsung Advanced Institute of Technology, Mt. 14-1, Nongseo-Dong, Giheung-Gu, Yongin-Si, Gyeonggi-Do 446-712, Republic of Korea

Received 9 November 2007; received in revised form 12 December 2007; accepted 12 December 2007
Available online 23 December 2007

Abstract

A transient three-dimensional, single-phase and non-isothermal numerical model of polymer electrolyte membrane (PEM) fuel cell with high operating temperature has been developed and implemented in computational fluid dynamic (CFD) code. The model accounts for transient convective and diffusive transport, and allows prediction of species concentration. Electrochemical charge double-layer effect is considered. Heat generation according to electrochemical reaction and ohmic loss are involved. Water transportation across membrane is ignored due to low water electro-osmosis drag force of polymer polybenzimidazole (PBI) membrane. The prediction shows transient in current density which overshoots (undershoots) the stabilized state value when cell voltage is abruptly decreased (increased). The result shows that the peak of overshoot (undershoot) is related with cathode air stoichiometric mass flow rate instead of anode hydrogen stoichiometric mass flow rate. Current is moved smoothly and there are no overshoot or undershoot with the influence of charge double-layer effect. The maximum temperature is located in cathode catalyst layer and both fuel cell average temperature and temperature deviation are increased with increasing of current load.
© 2007 Elsevier B.V. All rights reserved.

Keywords: Fuel cell; High operating temperature; Computational fluid dynamic; Charge double-layer

1. Introduction

Polymer electrolyte membrane (PEM) fuel cell is an electrochemical device in which energy of chemical reaction is converted into electricity directly. Useful features such as high power density, simple, safe construction and fast start-up make those particularly suitable for home appliance, vehicles and transportation tools [1]. Research and development of PEM fuel cell system have been increased dramatically in the past few years, and most of them are concerned with steady state condition. However, design and control of PEM fuel cell will also require a thorough understanding of its transient characteristics which are important for power conditioning in residential applications and for automotive systems. Although some dynamic characteristics can be determined from experiments, a model capable of predicting transient response is necessary so that system behavior can be analyzed by means of computer simulation in different conditions of load current, pressure of reactant gases, temperature and stack voltage, etc. Capability of predicting transient response is also proved useful for optimizing control schemes [2].

Prior to this work, a number of PEM fuel cell transient mathematical models were available in literature. Almost all these models were based on system-level which were simple and included all important characteristics of PEM fuel cell [3–9]. Cell voltage was modeled as a function of various contributing variables, such as current, cell temperature and partial pressure of oxygen at cathode inlet. Effects of ohmic resistance, over voltage and electrochemical charge double-layer capacitance were also considered. These studies established good basis for understanding transient response in PEM fuel cell. However, these models were not enough to understand intricate actual physical processes inside PEM fuel cell completely because transient behaviors of various properties were not included simultaneously, particularly the governing fundamental processes, such as gas transport through gas diffusion layer and effect of electrical conductivity. Recently, computational fluid dynamics (CFD) and improved transport models had made the development of more realistic computational models available [10–16]. Detail description of physical-chemical processes and coupled transport equations with electrochemical kinetics were included. Most of these models were focused

* Corresponding author. Tel.: +82 31 280 9363.
E-mail address: jie.peng@samsung.com (J. Peng).

0378-7753/$ – see front matter © 2007 Elsevier B.V. All rights reserved.
doi:10.1016/j.jpowsour.2007.12.042

Nomenclature

a	activity of gas species
A_{mem}	cell active area (m^2)
C_{df}	differential capacitance of porous catalyst layer ($F\,m^{-2}$)
C_{dl}	effective double-layer capacitance per unit geometric volume ($F\,m^{-3}$)
D_{kj}	binary-diffusion coefficient
E	sum of internal and kinetic energy (J)
E_A	active energy (J)
F	Faraday constant ($96487\,C\,mol^{-1}$)
h	enthalpy of gas species
i^{ref}	reference exchange current density ($A\,m^{-3}$)
i_0^{ref}	reference exchange current density at reference temperature ($A\,m^{-3}$)
I	local current density ($A\,m^{-2}$)
I_{avg}	average current density ($A\,m^{-2}$)
j	current density ($A\,m^{-3}$)
$\boldsymbol{J}$	diffusive mass flux vector
K	permeability of porous electrode (m^{-2})
M	molecular weight of gas species ($kg\,mol^{-1}$)
p	pressure (Pa)
R	universal gas constant ($8.314\,J\,mol^{-1}\,K^{-1}$)
ε	entropy ($J\,K^{-1}$)
$\boldsymbol{S}_u$	source term vector of momentum equation
S_m, S_k, S_h, S_{sol}, S_{mem}	source terms of continuity, species, energy and charge equation
t	time (s)
T	temperature (K)
T_0	reference temperature (393 K)
$\boldsymbol{u}$	gas flow velocity vector ($m\,s^{-1}$)
V_0	thermodynamic equilibrium potential (V)
V_{lk}	atomic diffusion volume
Y	mass fraction of gas species

Greek symbols

α	charge transfer coefficient
β	empirically determined concentration parameters
ε	porosity of the electrode materials
ϕ	potential (V)
η	local over potential (V)
κ	electrical (ionic) conductivity ($S\,m^{-1}$)
κ_0	pre-exponential factor ($S\,m^{-1}$)
λ	thermal conductivity ($W\,m^{-1}\,K^{-1}$)
λ_{eff}	effective thermal conductivity ($W\,m^{-1}\,K^{-1}$)
μ	dynamic viscosity ($kg\,s^{-1}\,m^{-2}$)
ρ	density of gas mixture ($kg\,m^{-3}$)
$\boldsymbol{\tau}$	viscous stress tensor
$\boldsymbol{\tau}_{eff}$	effective stress tensor
ξ_{ss}	specific surface area of porous catalyst layer ($m^3\,m^{-2}$)
ζ_i	constant number determined according to the experiment

Subscripts and superscripts

a	anode
c	cathode
f	fluid
H_2	hydrogen
H_2O	water
K	species
mem	membrane electrolyte phase
O_2	oxygen
s	solid
sol	electrode solid phase

on steady state behavior in order to facilitate the understanding of physical process and mechanism in PEM fuel cell. More recently, Shimpalee et al. [2] and Wang and Wang [17] extended the single-domain model of Um et al. [18] by considering all important transient processes occurred in PEM fuel cell. Transient response of cell was predicted in terms of local distribution of gas concentration and current density. However, effect of electrochemical charge double-layer was ignored according to theoretical estimation of various time constants where time constant of charge double-layer was sufficiently short to be ignored [17].

It has been known that in PEM fuel cell, charge double-layer is occurred in a thin layer on or near electrochemical reaction interface and acted as an electrical capacitor during transient procedure. Such capacitance is usually in the order of a few Farads, which is high in terms of capacitance value [19]. This charge double-layer can result in that cell current is moved gently and smoothly to new value in response to step change of cell operating condition.

In this paper, a complete transient numerical model capable of characterizing transient response of high temperature ($T \geq 393$ K) PEM fuel cell with polymer polybenzimidazole (PBI) membrane was proposed with incorporating capacitor effect of charge double-layer. Transient characteristics of PEM fuel cell were modeled by extending the three-dimensional model in previous paper [20] with accumulation (unsteady) term. Potential field equations were modified with considering about charge double-layer capacitance in electrochemical reaction interface based on macro-homogeneous theory of porous electrode [21,22]. Variation of charge double-layer capacitance with potential was ignored. All the important transient processes occurred in PEM fuel cell with high operating temperature, such as gas transport, species dispersion and charge double-layer discharge were considered comprehensively. In this study the PEM fuel cell was assumed to be operated at 433.15 K. Product water was assumed to be vaporous and treated as ideal gas. Water transportation across membrane was ignored due to low water electro-osmosis drag force in PBI membrane. The model was developed and implemented in the commercial CFD code FLUENT 6.1 with custom developed user-defined-functions (UDF) [23].

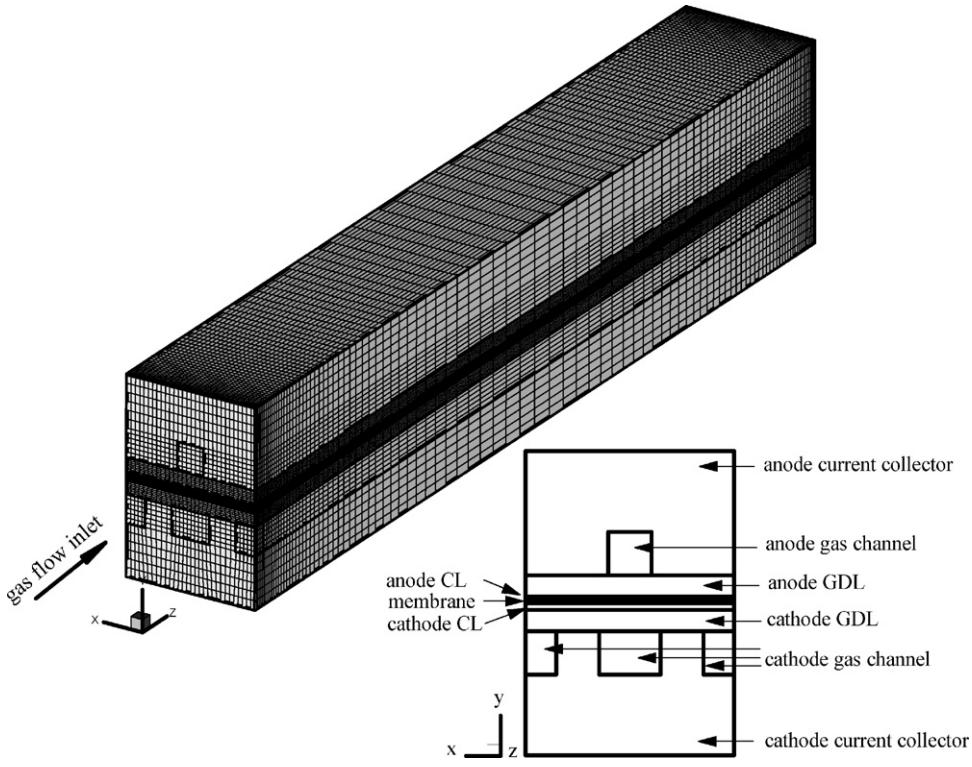

Fig. 1. Model schematic of a PEM fuel cell.

2. Mathematical model

Fig. 1 schematically shows that PEM fuel cell can be divided into following sub-regions: current collector, gas flow channel, gas diffusion layer (GDL) and catalyst layer (CL) in both anode and cathode sides, and membrane in the middle. Reactant feed is conveyed by gas flow channel and distributed to anode and cathode side. Then reactant is passed through respective porous GDL and reached CL where electrochemical reaction is occurred. The membrane acts as gas separator, electrolyte and proton conductor. Electrons are collected by anode current collector which is connected to cathode current collector through external circuit. In this study, anode feed is pure dry hydrogen and dry air is paralleled in cathode gas channel. Since gas streams in gas flow channel are at low velocity (or low Reynolds number), laminar flow with ideal gas behavior is assumed. Membrane is considered impermeable to gases. Product water is assumed to be vaporous and water transportation across membrane is ignored.

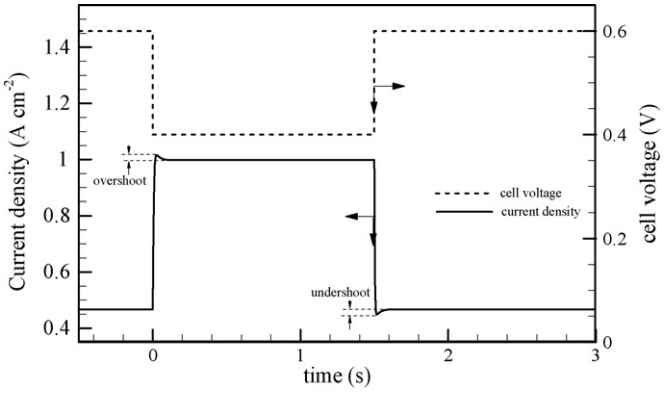

Fig. 2. Transient response of average current density while cell voltage changes between 0.6 and 0.4.

2.1. Governing equations

Governing equations based on the conservation laws of mass, momentum, species, energy and charge by extending the three-dimensional model of [20] with including time dependent analysis can be written, in vector form, as

$$\text{Continuity} \quad \varepsilon\frac{\partial\rho}{\partial t} + \nabla\cdot(\rho u) = S_{\mathrm{m}} \tag{1}$$

$$\text{Momentum} \quad \frac{1}{\varepsilon}\frac{\partial(\rho u)}{\partial t} + \frac{1}{\varepsilon^2}\nabla\cdot(\rho u u) = -\nabla p + \nabla\cdot\tau + S_{\mathrm{u}} \tag{2}$$

$$\text{Species} \quad \varepsilon\frac{\partial(\rho Y_k)}{\partial t} + \nabla\cdot(\rho u Y_k) = \nabla\cdot J_k + S_k \tag{3}$$

$$\text{Energy} \quad \frac{\partial(\rho E)}{\partial t} + \nabla\cdot(u(\rho E + p)) = \nabla\cdot\left(\lambda_{\mathrm{eff}}\nabla T - \sum_k h_k J_k + (\tau_{\mathrm{eff}}\cdot u)\right) + S_{\mathrm{h}} \tag{4}$$

$$\text{Charge} \quad -C_{\mathrm{dl}}\frac{\partial\eta}{\partial t} + \nabla\cdot(\kappa_{\mathrm{sol}}\nabla\phi_{\mathrm{sol}}) + S_{\mathrm{sol}} = 0 \tag{5}$$

$$C_{\mathrm{dl}}\frac{\partial \eta}{\partial t} + \nabla \cdot (\kappa_{\mathrm{mem}} \nabla \phi_{\mathrm{mem}}) + S_{\mathrm{mem}} = 0 \tag{6}$$

ρ is density of gas mixture, which is defined as

$$\rho = \frac{1}{\sum_k Y_k/\rho_k} \tag{7}$$

where ρ_k is density of species k and it can be calculated according to ideal gas law relation

$$\rho_k = \frac{pM_k}{RT} \tag{8}$$

$\boldsymbol{J}_k$ is diffusive mass flux vector, which can be written as

$$\boldsymbol{J}_k = -\sum_j \rho D_{kj} \nabla Y_j \tag{9}$$

D_{kj} is binary-diffusion coefficient which can be calculated according to the empirical expression [24]

$$D_{kj} = \frac{T^{1.75}(1/M_k + 1/M_j)^{1/2}}{p\left(\left(\sum_l V_{lk}\right)^{1/3} + \left(\sum_l V_{lj}\right)^{1/3}\right)^2} \times 10^{-3} \tag{10}$$

where V_{lk} is atomic diffusion volume and the value of $\sum V_{lk}$ is given by Cussler [24]. λ_{eff} is effective thermal conductivity in a porous material consisting of electrode solid matrix and gas, which is given by

$$\lambda_{\mathrm{eff}} = \varepsilon\lambda_{\mathrm{f}} + (1-\varepsilon)\lambda_{\mathrm{s}} \tag{11}$$

where λ_{s} is thermal conductivity of electrode solid matrix. λ_{f} is thermal conductivity of gas, which can be expressed as a polynomial function of temperature

$$\lambda_{\mathrm{f}} = \varsigma_0 + \varsigma_1 T + \varsigma_2 T^2 + \varsigma_3 T^3 \tag{12}$$

where ς_i, $i=0,\ldots,3$ can be determined according to experiment. Similar to the thermal conductivity, the viscosity and heat capacity of each gas species can also be described by polynomial expression of temperature with empirical coefficient. More details can be referred in [20].

Solid electrode phase potential ϕ_{sol} Eq. (5), which is solved in current collector, GDL and CL regions of both anode and cathode sides, accounts for electron transportation through electrode solid conductive materials. Membrane electrolyte phase potential ϕ_{mem} Eq. (6), which represents proton transportation through CL and membrane, is solved in membrane and CL regions. Charge double-layer effect is incorporated with time dependent term. The double-layer capacitance per unit geometric volume of electrochemical reaction porous electrode, C_{dl}, is given by [21]

$$C_{\mathrm{dl}} = \xi_{\mathrm{ss}} C_{\mathrm{df}} \tag{13}$$

where ξ_{ss} is specific surface area of CL which depends on its porous structure, and C_{df} is differential capacitance which depends on property of catalyst, such as catalyst loading [25]. As we have known that charge double-layer effect is occurred at the electrochemical reaction interface between electrolyte and electrode. In this study, C_{dl} is assumed to be homogeneous in CL of both anode and cathode sides, and the value of C_{dl} is zero in the regions except CL. η is local over-potential which can be expressed as

$$\eta_{\mathrm{a}} = \phi_{\mathrm{sol}} - \phi_{\mathrm{mem}} \tag{14}$$

$$\eta_{\mathrm{c}} = \phi_{\mathrm{sol}} - \phi_{\mathrm{mem}} - V_0 \tag{15}$$

V_0 is the thermodynamic equilibrium potential which can be given by [19]

$$V_0 = 1.17 - 2.756 \times 10^{-4}(T - 373.15) + 4.308 \times 10^{-5} \ln\left(\frac{a_{\mathrm{H_2}}(a_{\mathrm{O_2}})^{1/2}}{a_{\mathrm{H_2O}}}\right) \tag{16}$$

This equilibrium potential is calculated from thermodynamic data of reaction enthalpy and entropy changes while product water is assumed to be vaporous. Definitions of $a_{\mathrm{H_2}}$, $a_{\mathrm{O_2}}$ and $a_{\mathrm{H_2O}}$ are

$$a_{\mathrm{H_2}} = \frac{p_{\mathrm{H_2}}}{p^0_{\mathrm{H_2}}}, \quad a_{\mathrm{O_2}} = \frac{p_{\mathrm{O_2}}}{p^0_{\mathrm{O_2}}}, \quad a_{\mathrm{H_2O}} = \frac{p_{\mathrm{H_2O}}}{p^0_{\mathrm{H_2O}}} \tag{17}$$

where $p_{\mathrm{H_2}}$, $p_{\mathrm{O_2}}$ and $p_{\mathrm{H_2O}}$ are partial pressure of gas species.

Detail of various source terms in Eqs. (1)–(6) can be seen in Table 1. It shows that either generation or consumption of gas species and creation of electric current are occurred only in CL region where electrochemical reaction is taken place. Current densities at anode and cathode can be described by Butler–Volmer equation as [26]

$$j_{\mathrm{a}} = i_{\mathrm{a}}^{\mathrm{ref}} a_{\mathrm{H_2}}^{\beta_{\mathrm{H_2}}} \left[\exp\left(\frac{\alpha_{\mathrm{a}} F \eta_{\mathrm{a}}}{RT}\right) - \exp\left(-\frac{\alpha_{\mathrm{c}} F \eta_{\mathrm{a}}}{RT}\right)\right] \tag{18}$$

$$j_{\mathrm{c}} = i_{\mathrm{c}}^{\mathrm{ref}} a_{\mathrm{O_2}}^{\beta_{\mathrm{O_2}}} a_{\mathrm{H_2O}}^{\beta_{\mathrm{H_2O}}} \left[\exp\left(-\frac{\alpha_{\mathrm{c}} F \eta_{\mathrm{c}}}{RT}\right) - \exp\left(\frac{\alpha_{\mathrm{a}} F \eta_{\mathrm{c}}}{RT}\right)\right] \tag{19}$$

where α_{a} and α_{c} are anodic and cathodic charge transfer coefficients, see in Table 2. $i_{\mathrm{a}}^{\mathrm{ref}}$ and $i_{\mathrm{c}}^{\mathrm{ref}}$ are reference exchange current densities which depend on local temperature,

$$i_{\mathrm{a}}^{\mathrm{ref}} = i_{\mathrm{a},0}^{\mathrm{ref}} \exp\left[-\frac{E_{\mathrm{A,a}}}{R}\left(\frac{1}{T} - \frac{1}{T_0}\right)\right] \tag{20}$$

$$i_{\mathrm{c}}^{\mathrm{ref}} = i_{\mathrm{c},0}^{\mathrm{ref}} \exp\left[-\frac{E_{\mathrm{A,c}}}{R}\left(\frac{1}{T} - \frac{1}{T_0}\right)\right] \tag{21}$$

where $E_{\mathrm{A,a}}$ and $E_{\mathrm{A,c}}$ are active energies [22]. $i_{\mathrm{a},0}^{\mathrm{ref}}$ and $i_{\mathrm{c},0}^{\mathrm{ref}}$ are reference exchange current densities at reference temperature T_0. $\beta_{\mathrm{H_2}}$, $\beta_{\mathrm{O_2}}$ and $\beta_{\mathrm{H_2O}}$ are empirically determined concentration parameters for $\beta_{\mathrm{H_2}} = 0.25$, $\beta_{\mathrm{O_2}} = 0.5$ and $\beta_{\mathrm{H_2O}} = 0.25$. Local current density $\boldsymbol{I}$ in membrane, according to Ohm's law, is defined as

$$\boldsymbol{I} = -\kappa_{\mathrm{mem}} \nabla \phi_{\mathrm{mem}} \tag{22}$$

Temperature dependence of membrane ionic conductivity can be accurately described by Arrhenius equations [27]

$$\kappa_{\mathrm{mem}} = \kappa_0 \exp\left[-\frac{E_{\mathrm{A},\kappa}}{R}\left(\frac{1}{T} - \frac{1}{T_0}\right)\right], \tag{23}$$

where $E_{\mathrm{A},\kappa}$ is activation energy and κ_0 is pre-exponential factor at reference T_0. Average current density, which is the average

Table 1
Source terms for governing equations in various regions of a polymer electrolyte fuel cell

	Source terms			
	Flow channels	GDL	CL	Membrane
Continuity	$S_{m,a} = S_{m,c} = 0$	$S_{m,a} = S_{m,c} = 0$	$S_{m,a} = -\frac{M_{H_2}}{2F} j_a$ $S_{m,c} = -\frac{M_{O_2}}{4F} j_c + \frac{M_{H_2O}}{2F} j_c$	–
Momentum	$\boldsymbol{S}_{u,a} = \boldsymbol{S}_{u,c} = 0$	$\boldsymbol{S}_{u,a} = \boldsymbol{S}_{u,c} = -\frac{\mu}{K_{GDL}}\boldsymbol{u}$	$\boldsymbol{S}_{u,a} = \boldsymbol{S}_{u,c} = -\frac{\mu}{K_{CL}}\boldsymbol{u}$	–
Species	$S_{k,a} = S_{k,c} = 0$	$S_{k,a} = S_{k,c} = 0$	$S_{H_2,a} = -\frac{M_{H_2}}{2F} j_a$ $S_{O_2,c} = -\frac{M_{O_2}}{4F} j_c$ $S_{H_2O,c} = -\frac{M_{H_2O}}{2F} j_c$	–
Energy	$S_{h,a} = S_{h,c} = 0$	$S_{h,a} = S_{h,c} = 0$	$S_{h,a} = 0$ $S_{h,c} = \frac{\lvert j_c \rvert}{2F} T\lvert\Delta s\rvert + \lvert j_c \eta_c \rvert$	$S_h = \frac{I^2}{\kappa_{mem}}$
Charge	$S_{sol,a} = S_{sol,c} = 0$	$S_{sol,a} = S_{sol,c} = 0$	$S_{sol,a} = -j_a$ $S_{sol,c} = j_c$	$S_{sol} = 0$
	$S_{mem,a} = S_{mem,c} = 0$	$S_{mem,a} = S_{mem,c} 0$	$S_{mem,a} = j_a$ $S_{mem,c} = -j_c$	$S_{mem} = 0$

value of local current density in normal direction over entire membrane, can be obtained by

$$I_{avg} = \frac{1}{A_{mem}} \int_{A_{mem}} \boldsymbol{I} \cdot \mathrm{d}A, \tag{24}$$

where A_{mem} is cell active area.

The heat released from CL is caused by enthalpy change and irreversibility related to charge transfer [15]. In this paper, ohmic heating is ignored in current collector, GDL and CL but considered in membrane due to its relatively low ionic conductivity. Empirically, change of entropy Δs, as a function of temperature T, can be expressed as [19]

$$\Delta s = 33.64 + 4.52564 \times 10^{-2} T - 2.98397 \times 10^{-5} T^2 + 3.40625 \times 10^{-9} T^3 - 2.60417 \times 10^{-12} T^4 \tag{25}$$

which is valid for temperature from 373 to 1137 K.

Table 2
Electrochemical properties

Parameter	Symbol	Value	Unit
Porosity of GDL	ε	0.8	–
Porosity of CL	ε	0.6	–
GDL/CL hydraulic permeability		5.0e-12	m^{-2}
Membrane ionic conductivity	κ_0	12.99	$S\,m^{-1}$
GDL/CL electric conductivity	κ	103.3	$S\,m^{-1}$
Current collector electric conductivity	κ	535	$S\,m^{-1}$
Anodic charge transfer coefficient	α_a	1.0	–
Cathodic charge transfer coefficient	α_c	1.0	–
Anode reference exchange current density	$i^{ref}_{a,0}$	1.0e8	$A\,m^{-3}$
Cathode reference exchange current density	$i^{ref}_{c,0}$	1.5e2	$A\,m^{-3}$
Thermal conductivity of CL		1.7	$W\,m^{-1}\,K^{-1}$
Thermal conductivity of membrane		0.95	$W\,m^{-1}\,K^{-1}$
Thermal conductivity of GDL		1.7	$W\,m^{-1}\,K^{-1}$
Thermal conductivity of current collector		25	$W\,m^{-1}\,K^{-1}$

2.2. Boundary and initial conditions

Eqs. (1)–(6) form a complete set of governing equations. The corresponding boundary and initial conditions were described as follows.

(1) On gas channel inlet boundaries, stoichiometric mass flow rate and mass fractions of species were prescribed according to the current with cell voltage of 0.4 V. On outlet boundaries, pressure boundary conditions were applied with cell operating pressure value of 1.1 atm.
(2) In Fig. 1, on both anode and cathode external boundaries normal to y-axis, which contact with external electrical circuit, electrical current was generated only through these boundaries. Step change of cell operating voltage between 0.4 and 0.6 V was applied.

Table 3
Geometrical and operating parameters

Parameter	Value	Unit
Cell width	3.4	mm
Channel length	235	mm
Channel height	0.7	mm
Anode channel width	0.7	mm
Cathode channel width	1.0	mm
Anode GDL thickness	0.34	mm
Anode CL thickness	0.04	mm
Membrane thickness	0.065	mm
Cathode CL thickness	0.11	mm
Cathode GDL thickness	0.34	mm
Thickness of current collector (both anode and cathode)	2	mm
Operating temperature	433	K
Anode stoichiometric mass flow rate	1.5	–
Cathode stoichiometric mass flow rate	2.0	–
Anode outlet pressure	1.1	atm
Cathode outlet pressure	1.1	atm
Anode inlet mass fraction H_2	1.0	–
Cathode inlet mass fraction O_2:N_2	0.22:0.78	–

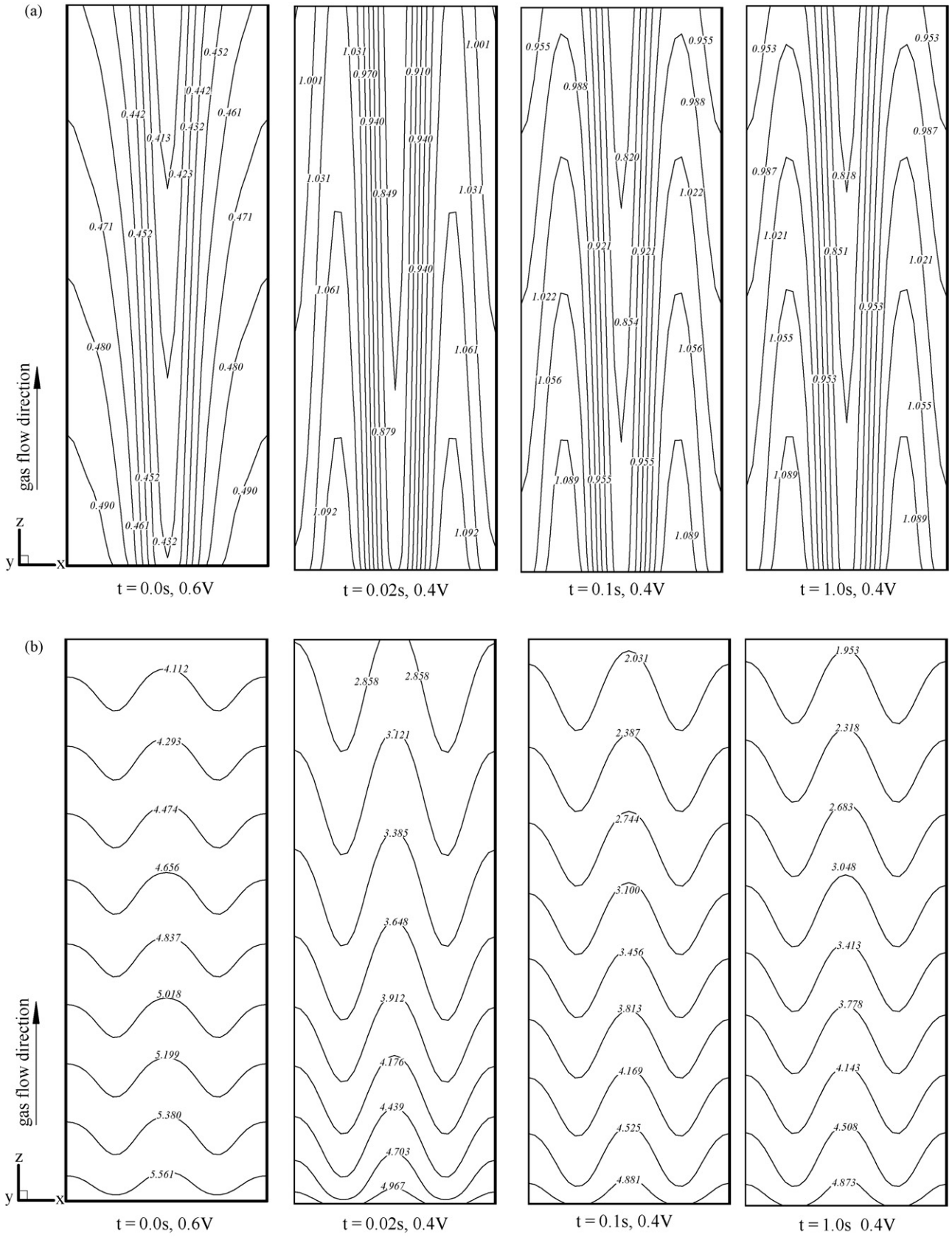

Fig. 3. (a) Local transient current density contour (unit: A cm^{-2}) and (b) local transient oxygen mole concentration contour (unit: mol m^{-3}) at different times while cell voltage changes from 0.6 to 0.4.

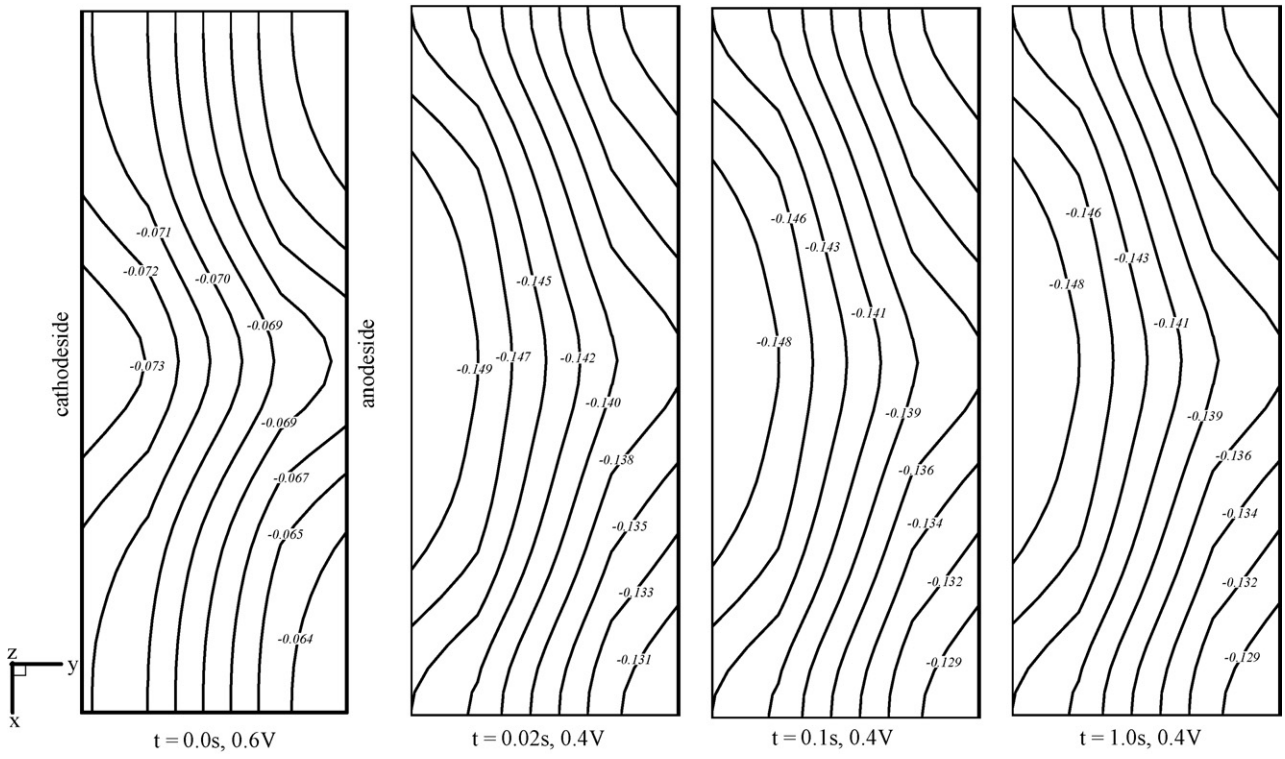

Fig. 4. Local transient membrane potential contour at different times while cell voltage changes from 0.6 to 0.4 (unit: V).

(3) Zero flux of ϕ_{sol} was defined on interface between CL and membrane. Zero flux of ϕ_{mem} was defined on interface between GDL and CL.
(4) In isothermal case, cell temperature was assumed to be constant with value of 433.15 K. In non-isothermal case, inlet gas was assumed to be pre-heated with temperature 433.15 K and outside environment temperature was also set to be 433.15 K.
(5) As shown in Fig. 1, the fuel cell with single straight gas channel was employed. Generally, fuel cell flow plate was formed with a plurality of gas channels. Therefore, symmetrical boundary condition was applied on the side surfaces normal to x-axis. No-slip boundary condition was applied on remaining walls.
(6) The initial conditions were applied with the steady-state fields for cell operating voltage of 0.6 V.

2.3. Numerical procedure

The numerical procedure was based on the commercial flow solver FLUENT 6.1. Volumetric sources or sinks in Table 1 were implemented in the solver with custom developed user-defined-function (UDF). Eqs. (1)–(6) were solved in fully implicit scheme with second-order precision for both spatial and temporal discretization. Therefore, the numerical procedure was

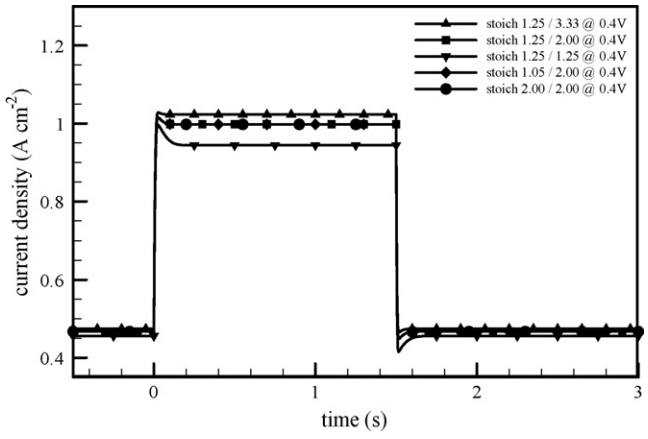

Fig. 5. Transient response of average current density while cell voltage changes between 0.6 and 0.4 with different anode and cathode stoichimometric mass flow rate.

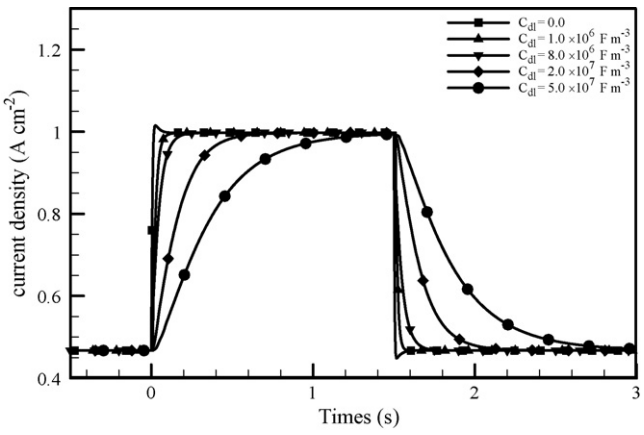

Fig. 6. Transient response of average current density while cell voltage changes between 0.6 and 0.4 with effect of charge double-layer.

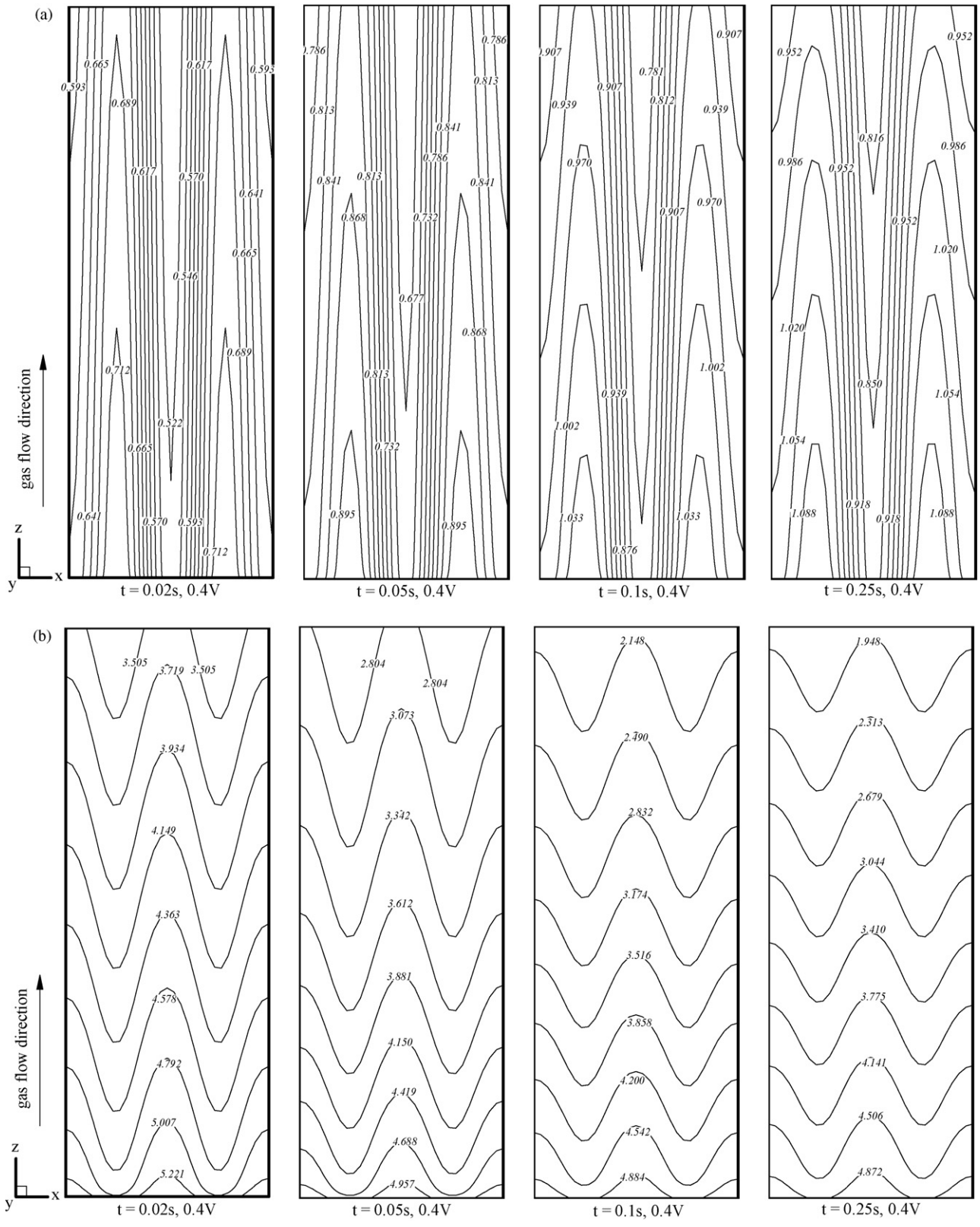

Fig. 7. (a) Local transient current density contour (unit: A cm^{-2}) and (b) local transient oxygen mole concentration contour (unit: mol m^{-3}) at different times while the cell voltage changes from 0.6 to 0.4 with double-layer effect considered and the value of C_{dl} is 8.0×10^6 F m^{-3}.

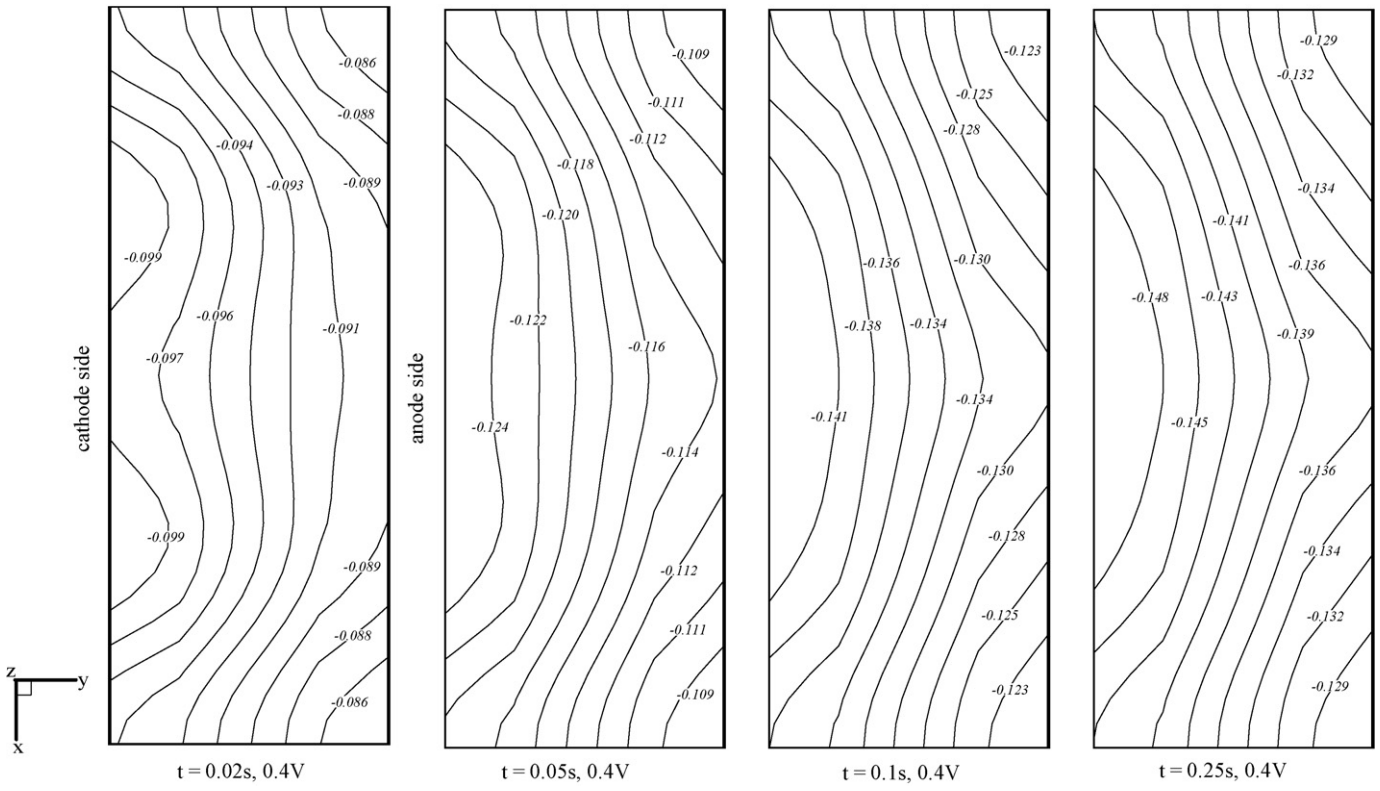

Fig. 8. Local transient membrane potential contour at different times while cell voltage changes from 0.6 to 0.4 with double-layer considered and the value of C_{dl} is 8.0×10^6 F m^{-3} (unit: V).

stable throughout the time step Δt. Note, that in this paper, several values of Δt had been tested in order to make sure that the results were independent of time step size. Furthermore, stringent numerical tests were performed during steady state simulations to ensure that the solutions were independent of grid size. A mesh with about 180,000 grid points and a time step size Δt of 0.005 s were found to provide sufficient spatial and temporal resolution.

3. Results and discussion

As shown in Fig. 1, a single-channel PEM fuel cell with polymer polybenzimidazole (PBI) membrane is chosen for a parametric study. Values of relative parameters can be found in Table 3.

3.1. Overshoot and undershoot

Generally, overshoot or undershoot of current density is found during step change in cell operating condition, such as cell voltage. It is caused by the fact that change of local gas concentration is always delayed behind change of local potential.

Fig. 2 shows response in average current density to one time step change in cell voltage without considering about the influence of charge double-layer. When cell voltage is changed in one time from 0.6 to 0.4 V at $t = 0.0$ s, overshoot is occurred. The average current density is rapidly increased from 0.467 to 1.016 A cm^{-2}, then decreased with time and stabilized with value of 0.997 A cm^{-2}. When cell voltage is changed in one time from 0.4 back to 0.6 V at $t = 1.5$ s, undershoot is occurred oppositely. The average current density is rapidly decreased from 0.997 to 0.448 A cm^{-2}, then increased with time and finally stabilized with value of 0.467 A cm^{-2}. Fig. 3(a) shows local current density distribution on intermediate cross-section of membrane at four different time steps while cell voltage is changed from 0.6 to 0.4 V. At initial sate corresponding to cell voltage of 0.6 V at time $t = 0.0$ s, the local current density near gas inlet side is high and decreased along gas flow direction. Since the stoichiometric mass flow rate of anode and cathode sides are prescribed as 1.25 and 2.0 when cell is operated at voltage of 0.4 V, it corresponds to stoichiometric mass flow rate of 2.7 and 4.3 at cell voltage of 0.6 V. We have large excess amount of fuel and air at time $t = 0.0$ s. Therefore, the current density distribution across membrane is distinctively different from those (Fig. 3(a)) in [20]. Variation is small over entire cell active area. The maximum and minimum local current densities are 0.490 and 0.413 A cm^{-2}, respectively. When cell voltage is dropped to 0.4 V in 0.02 s, the local current density is significantly increased over entire cell active area and the contour pattern is distinctively different from that at $t = 0.0$ s. The highest local current density is 1.092 A cm^{-2} which is located under current collector land area near gas inlet side because of the influence of gas concentration and ohmic losses in CL and GDL. The lowest value is 0.849 A cm^{-2} and located under gas channel near gas outlet side. As time increases, local current density is decreased while the distribution contour pattern is similar to that at $t = 0.02$ s. At time $t = 1.0$ s, when it is stabilized, the highest local current density is 1.089 A cm^{-2} and the lowest value is 0.818 A cm^{-2}.

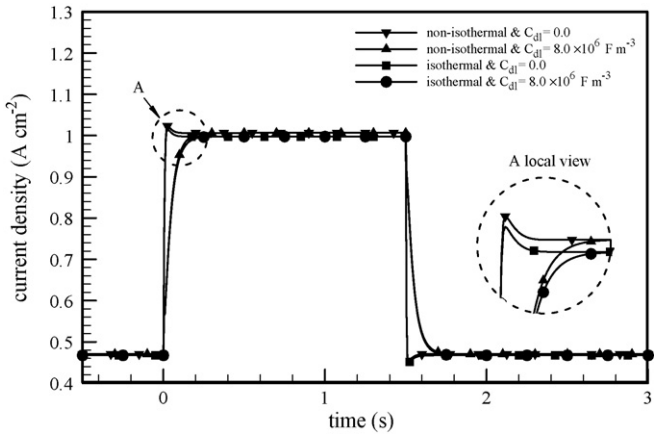

Fig. 9. Transient response of average current density while cell voltage changes between 0.6 and 0.4 with non-isothermal model.

Fig. 3(b) shows transient local oxygen mole concentration contours on intermediate cross-section of cathode catalyst layer. It can be seen that local oxygen mole concentration distribution is consistent with the distribution of local current density. Mole concentration of oxygen is decreased monotonically along gas flow direction. The concentration value under current collector land area is smaller than that under gas channel due to gas diffusion and consumption. When cell voltage is dropped to 0.4 V in 0.02 s, it can be seen that oxygen is depleted rapidly towards gas outlet side and the concentration distribution becomes much more non-uniform. As time increases, the oxygen concentration is decreased gradually especially in region near gas outlet side. Oxygen mole concentration variation over entire cathode CL is increased from 1.50 mol m^{-3} at t = 0.0 s to 2.95 mol m^{-3} at t = 1.0 s. The oxygen mole concentration near gas inlet side is stabilized with 12.4% reduction, whereas 52.5% reduction near gas outlet side.

When cell voltage is changed from 0.4 back to 0.6 V at t = 1.5 s, on the contrary to Fig. 3(a), local current density is significantly decreased over entire cell active area suddenly, and then increased. Variation of local current density over entire cell active area is decreased. This is caused by the facts that oxygen distribution variation is decreased since stoichiometric mass flow rate is increased from 1.25 and 2.0 (at 0.4 V) to 2.7 and 4.3 (at 0.6 V).

Fig. 4 shows membrane electrolyte phase potential contours at midway cross-section area of membrane. Due to the non-uniform local current production in adjacent CL, there are gradients in both x and y directions. Since charge double-layer effect is not considered at this moment, it can be seen that electrolyte phase potential distribution can be stabilized much more promptly than oxygen concentration.

Fig. 5 presents the influence of gas stoichimometric mass flow rate on cell transient response. When stoichiometric mass flow rate of air is increased form 2.00 to 3.33 at cell voltage of 0.4 V, average current density is increased and peaks of current overshoot and undershoot are reduced at the same time. In contrast, when stoichiometric mass flow rate of air is decreased form 2.00 to 1.25 at cell voltage of 0.4 V, average current density is decreased while peaks of current overshoot and undershoot are enlarged. Moreover, form the result, it can be seen that stoichiometric mass flow rate of hydrogen does not influence the cell dynamic performance. This is caused by the fact that anode side is fed with pure dry hydrogen. It is distinctively different from [2], where the water activity in anode side is considered.

3.2. Double-layer effect

Charge double-layer is a complex electrode phenomenon. In electrochemical systems, a layer of charge on or near electrode/electrolyte interface is a store of electrical charge and energy, and behaves like an electrical capacitor [19]. In Eq. (13), the double-layer capacitance per unit geometric volume is proportional to specific surface area and differential capacitance. The specific surface area ξ_{ss} depends on porous structure of porous CL electrode and the differential capacitance C_{df} depends on catalyst content. In this study, value of ξ_{ss} is set to be 4125 m^2 cm^{-3} [28] and value of C_{df} is varied from 2×10^{-2} μF cm^{-2} and 2 μF cm^{-2} [29]. Therefore, according to Eq. (13), value of C_{dl} is set to vary from 8.25×10^5 F m^{-3} to 8.25×10^7 F m^{-3}. In this paper, property of both anode and cathode CL electrodes are assumed to be identical. This is not necessary, and one might identify cases where non-identical electrodes are desirable.

Fig. 6 shows the influence of charge double-layer on cell transient response. It can be seen that current is moved smoothly with increasing value of C_{dl}. From prior research [17,21], it is well known that time constant for double-layer charging is proportional to value of C_{dl}. Therefore, it takes much more time for the cell with large value of C_{dl} to stabilize after cell voltage is changed. From Fig. 6, it can be seen that value of current density at stabilized state is independent from C_{dl}. It means that charge double-layer just influences cell transient response and does not influence cell steady performance.

Fig. 7(a) shows local current density distribution on intermediate cross-section of membrane at four different time steps while cell voltage is changed from 0.6 to 0.4 V. Effect of charge double-layer is considered with C_{dl} value of 8.0×10^6 F m^{-3}. Since charge double-layer just influences cell transient response, the local transient current density contour will be same to those in

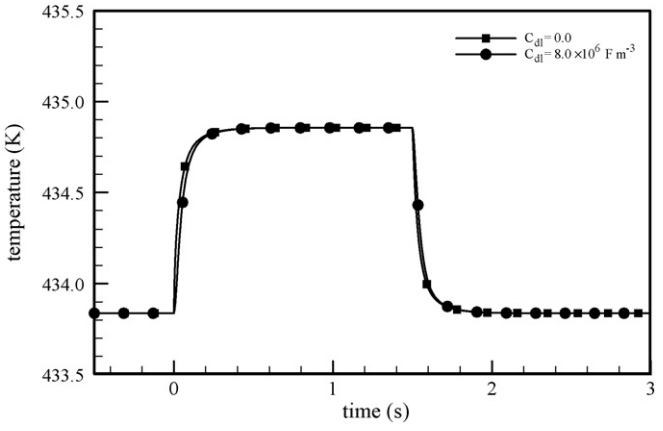

Fig. 10. Transient response of average temperature of membrane while cell voltage changes between 0.6 and 0.4.

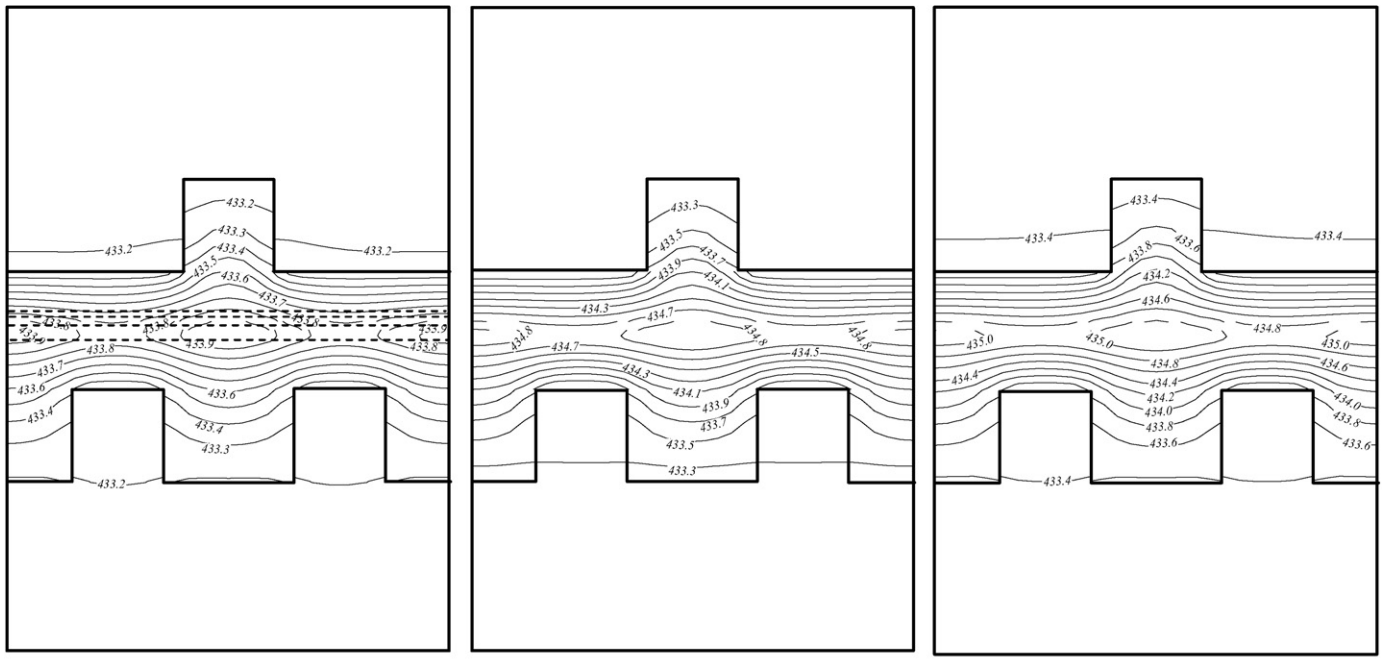

Fig. 11. Temperature distribution contour on midway section at different times while cell voltage changes from 0.6 to 0.4 without considering about charge double-layer (unit: K).

Fig. 3(a) at time $t = 0.0$ s with cell voltage 0.6 V. At time $t = 0.02$ s and cell voltage of 0.4 V, comparing with Fig. 3, due to influence of charge double-layer, current density is increased more slowly and the variation is smaller than those without considering about charge double-layer. The maximum and minimum local current densities are 0.712 A cm^{-2} and 0.522 A cm^{-2}. As time increases, local current density is increased smoothly and the value near gas inlet side is increased faster than that near gas outlet side. In Fig. 7(b), as local current density is increased smoothly due to charge double-layer effect, oxygen mole concentration is decreased also smoothly and the value near gas inlet side is decreased more slowly than that near gas outlet side.

Fig. 8 presents membrane electrolyte phase potential contours at midway cross-section area of membrane corresponding to current density of Fig. 7(a). At time $t = 0.02$ s, distribution contour pattern is distinctively different from that in Fig. 4, which is caused by charging of charge double-layer. As time increases, absolute value of membrane potential is increased and the distribution contour pattern is become similar to those of steady state gradually.

3.3. Temperature response

In previous sections, the PEM fuel cell is assumed to be operated at constant temperature with value of 433.15 K. In real PEM fuel cell, heat is released from cathode catalyst layer due to electrochemical reaction and from membrane due to ohmic loss. Therefore, change of current load will lead to change of cell temperature. Fig. 9 shows response in average current density to step change in cell voltage with considering about heat transfer. Comparison with isothermal model, average current density of steady state at time $t = 1.0$ s is increased from 0.997 A cm^{-2} to 1.006 A cm^{-2}. It is clear from these result profiles that increasing load current will lead to increase cell temperature. As the results, cell performance will be improved due to the facts that membrane ionic conductivity will be increased with increasing of cell temperature [20]. Fig. 10 shows response in average temperature of membrane to step change in cell voltage. The temperature is moved smoothly even if charge double-layer effect is not considered. It shows that charge double-layer almost has no effects on transient response of cell temperature. Fig. 11 presents temperature distribution on midway section of cell for three time steps while cell voltage is changed from 0.6 to 0.4 V. It shows that the maximum temperature is located in cathode CL and the temperature deviation is increased with increasing of current load.

4. Conclusion

In this paper, a three-dimensional transient model of high temperature PEM fuel cell was presented to study the intricate transient response to step change in cell voltage. Effects of electrochemical charge double-layer, gas transport, and temperature influence on membrane ionic conductivity were considered. A single-channel PEM fuel cell with PBI membrane was adopted for parametric study. The contour of local current density, oxygen mole concentration and electrolyte phase potential were presented and discussed.

The results show that for the particular operating conditions and property parameters used in this study, when charge double-layer effect is not considered, current overshoot or undershoot can be found with step change of cell voltage. Peaks of over-

shoot and undershoot depend on air stoichiometry of cathode side, which can be reduced by increasing the value of air stoichiometry. Current density is moved smoothly and there is no overshoot or undershoot, while charge double-layer effect is considered with certain value of specific surface and differential capacitance of porous CL. Transient response of temperature is moved smoothly and charge double-layer has no effects on it. The maximum temperature is located in cathode CL and temperature deviation is increased with increasing of current load. These transient responses of PEM fuel cell captured herein for the first time, including charge double-layer and thermal effects on output current, are expected to be useful for design of power electronics and control algorithm for fuel cell systems.

References

[1] S. Srinivasan, R. Mosdale, P. Stevens, C. Yang, Rev. Energy Environ. 24 (1999) 281–328.
[2] S. Shimpalee, W.-k. Lee, J.W. Van Zee, H. Naseri-Neshat, J. Power Sources 156 (2006) 355–368.
[3] J.C. Amphlett, R.F. Mann, B.A. Peppley, P.R. Roberge, A. Rodrigues, J. Power Sources 61 (1996) 183–188.
[4] M. Wohr, K. Blowin, W. Schnurnberger, M. Fischer, W. Neubrand, G. Eigenberger, Int. J. Hydrogen Energy 23 (1998) 213–218.
[5] S. Yerramalla, A. Davari, A. Feliachi, T. Biswas, J. Power Sources 124 (2003) 104–113.
[6] M.J. Khan, M.T. Lqbal, Fuel cell 5 (1) (2005) 97–104.
[7] P.R. Pathapati, X. Xue, J. Tang, Renew. Energy 30 (2005) 1–22.
[8] D. Yu, S. Yuvarajan, J. Power Sources 142 (2005) 238–242.
[9] C.S. Wang, M.H. Nehrir, S.R. Shaw, IEEE Trans. Energy Convers. 20 (2) (2005) 442–451.
[10] D. Singh, D.M. Lu, N. Djilali, Int. J. Eng. Sci. 37 (4) (1999) 431–452.
[11] S. Um, C.Y. Wang, C.S. Chen, J. Electrochem. Soc. 147 (12) (2000) 4485–4493.
[12] T. Zhou, H. Liu, Int. J. Transport Phenom. 3 (2001) 177–198.
[13] T. Berning, D.M. Lu, N. Djilali, J. Power Sources 106 (2002) 284–294.
[14] P.T. Nguyen, T. Berning, N. Djilali, J. Power Sources 130 (1/2) (2004) 149–157.
[15] B.R. Sivertsen, N. Djilali, J. Power Sources 141 (2005) 65–78.
[16] Y. Wang, C.Y. Wang, J. Electrochem. Soc. 152 (2) (2005) A445–A453.
[17] Y. Wang, C.Y. Wang, Electrochim. Acta 50 (2005) 1307–1315.
[18] S. Um, C.Y. Wang, K.S. Chen, J. Electrochem. Soc. 147 (2000) 4485–4493.
[19] J. Larminie, A. Dicks, Fuel Cell Systems Explained, John Wiley and Sons Ltd., 2000, pp. 28–36.
[20] J. Peng, S.J. Lee, J. Power Sources 162 (2006) 1182–1191.
[21] B. Pillay, J. Newman, J. Electrochem. Soc. 143 (1996) 1806–1814.
[22] H. Ju, H. Meng, C.Y. Wang, Int. J. Heat Mass Trans. 48 (2005) 1303–1315.
[23] Fluent Incorporated, Fluent 6.0 and 6.1 User's Guide, 2001.
[24] E.L. Cussler, Diffusion Mass Transfer in Fluid Systems, second ed., Cambridge University Press, New York, USA, 1997.
[25] Y. Wang, J.P. Zheng, Rare Met. 25 (2006) 12–18.
[26] J.D.J. VanderSteen, B. Kenney, J.G. Pharoah, K. Karan, Proceedings of the Canadian Hydrogen and Fuel Cells Conference, September, 2004.
[27] Y.L. Ma, J.S. Wainright, M.H. Litt, R.F. Savinell, J. Electrochem. Soc. 151 (2004) A8–A16.
[28] Z.H. Teng, G. Wang, B. Yu, Y. Gao, J. Power Sources 164 (2007) 105–110.
[29] Yu.V. Pleskov, Yu.E. Evstefeeva, A.M. Baranov, Diamond Relat. Mater. 11 (2002) 1518–1522.